Second-Sphere Amino Acids Contribute to Transition-State Structure in Bovine Purine Nucleoside Phosphorylase†

Lei Li, Minkui Luo, Mahmoud Ghanem, Erika A. Taylor,‡ and Vern L. Schramm*

Department of Biochemistry, Albert Einstein College of Medicine, 1300 Morris Park Avenue, Bronx, New York 10461

Received October 23, 2007; Revised Manuscript Received December 4, 2007

ABSTRACT: Transition-state structures of human and bovine of purine nucleoside phosphorylases differ, despite 87% homologous amino acid sequences. Human PNP (HsPNP) has a fully dissociated transition state, while that for bovine PNP (BtPNP) has early S_N1 character. Crystal structures and sequence alignment indicate that the active sites of these enzymes are the same within crystallographic analysis, but residues in the second-sphere from the active sites differ significantly. Residues in BtPNP have been mutated toward HsPNP, resulting in double (Asn123Lys; Arg210Gln) and triple mutant PNPs (Val39Thr; Asn123Lys; Arg210Gln). Steady-state kinetic studies indicated unchanged catalytic activity, while pre-steady-state studies indicate that the chemical step is slower in the triple mutant. The mutant enzymes have higher affinity for inhibitors that are mimics of a late dissociative transition state. Kinetic isotope effects (KIEs) and computational chemistry were used to identify the transition-state structure of the triple mutant. Intrinsic KIEs from [1′-^{3}H], [1′-^{14}C], [2′-^{3}H], [5′-^{3}H], and [9-^{15}N] inosines were 1.221, 1.035, 1.073, 1.062 and 1.025, respectively. The primary intrinsic [1′-^{14}C] and [9-^{15}N] KIEs indicate a highly dissociative S_N1 transition state with low bond order to the leaving group, a transition state different from the native enzyme. The [1′-^{14}C] KIE suggests significant nucleophilic participation at the transition state. The transition-state structure of triple mutant PNP is altered as a consequence of the amino acids in the second sphere from the catalytic site. These residues are implicated in linking the dynamic motion of the protein to formation of the transition state.

Purine nucleoside phosphorylase (PNP,[1] E.C. 2.4.2.1) catalyzes the phosphorolysis of the N-ribosidic bonds of 6-oxypurine nucleosides and deoxynucleosides. The rate-limiting step for mammalian PNPs in the phosphorolysis reaction is release of the purine base (*1*). Transition-state analysis for PNPs from the human, bovine and *Plasmodium falciparum* enzymes reveals a unique transition-state structure for bovine PNP (*2*−*4*). While the intrinsic [1′-^{14}C] kinetic isotope effects are unity for human and *Plasmodium falciparum* PNPs, consistent with fully dissociated S_N1 transition states, that for bovine PNP is 1.022, indicating an early dissociative mechanism for bovine PNP (Figure 1) (*2*, *3*).

The amino acid sequences of human PNP (HsPNP) and bovine PNP (BtPNP) share 87% identity overall and are completely conserved at the catalytic sites (Figure 2), while their transition states are different (*2*, *4*). Structural comparison of the catalytic sites with both early and late transition state analogue inhibitors reveals no significant changes to suggest differences in these transition states (Figure 3; *5*, *6*). Structural and sequence comparisons reveal significant differences in amino acids at the subunit interface and in the second sphere from the surface of the proteins. Twenty-two of the thirty-three nonconserved residues are located on the surface of the proteins. Residues not located on the surface were examined for their distance from the active site (Table 1). Of these, residues 39, 123, and 210 of BtPNP are highly dissimilar and are 10−14 Å from the active site. A double mutant (Asn123Lys and Arg210Gln) and a triple mutant BtPNP (Val39Thr, Asn123Lys, and Arg210Gln) were created, with these residues being changed to those found in HsPNP. The purpose of these changes was to test the hypothesis that changes remote from the catalytic site could alter the transition state of the bovine enzyme to become more like HsPNP. Inhibition and kinetic isotope effect studies were conducted to characterize the chimeric proteins for comparison with the parent enzymes. The results establish that transition-state structure of BtPNP can be altered by remote mutations and implicate dynamic contribution to transition-state structure.

MATERIALS AND METHODS

Enzymes and Reagents. The reagents and enzymes used in the synthesis of isotopically labeled inosines have been described (*4*, *7*−*9*). All chemicals were the highest quality available and were purchased from commercial sources as described previously (*1*, *7*).

Mutagenesis, Transformation and Expression. The cDNAs were obtained from DNA 2.0 Inc., with nucleotide sequences optimized for expression in *Escherichia coli*. A thrombin cleavable 6-His tag was encoded at the N-terminus of the

† This work was supported by NIH Research Grants GM41916 and GM068036.

* Corresponding author. Tel: (718) 430-2813. Fax: (718) 430−8565. E-mail: vern@aecom.yu.edu.

‡ Current address: Department of Chemistry, Wesleyan University, Middletown, CT.

[1] Abbreviations: PNP, purine nucleoside phosphorylase; KIE, kinetic isotope effect; LB, Luria broth; DADMe-ImmH, 4′-deaza-1′-aza-2′-deoxy-1′-(9-methylene)-immucillin-H; ImmH, immucillin-H; ImmG, immucillin-G; DADMe-ImmG, 4′-deaza-1′-aza-2′-deoxy-1′-(9-methylene)-immucillin-G; Ni-NTA agarose, nickel-nitrilotriacetic acid agarose; Hepes, 4-(2-hydroxyethyl)-1-piperazineethanesulfonic acid.

10.1021/bi7021365 CCC: $40.75
Published on Web 02/19/2008

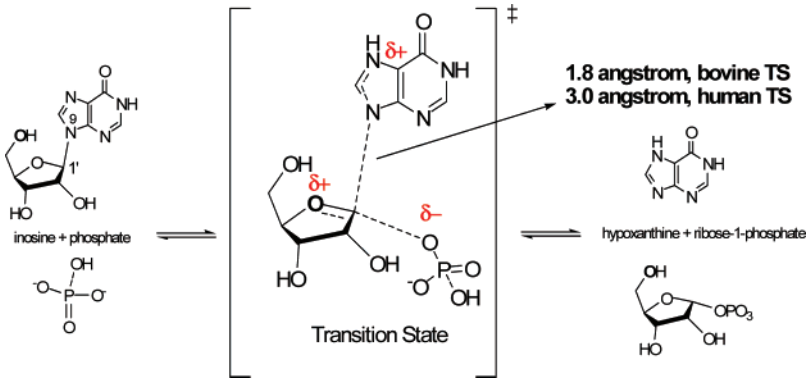

FIGURE 1: The reported transition states of human and bovine PNPs (*1*, *2*, *4*).

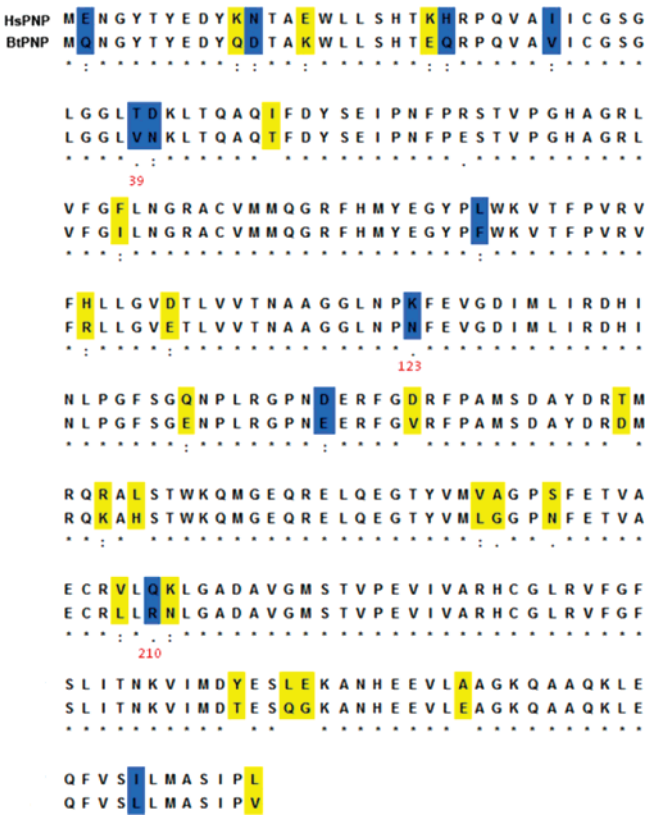

FIGURE 2: Sequence comparison of bovine and human PNPs. Residues that are not conserved between the two enzymes are highlighted (yellow for surface residues and blue for residues located within the proteins).

genes, which were subcloned into the pDNR vector. The plasmids were inserted into the pBAD-DEST49 vector by LR clonase II, and the resulting plasmids were transformed into XL-Blue competent cells. The sequences of the plasmids were verified by automated DNA sequencing. The recombinant plasmids were transformed into BL21A.I.(DE3) competent cells and plated onto LB/agar plates containing 100 μg/mL ampicillin. Single colonies were inoculated into 50 mL of LB containing 100 μg/mL ampicillin with shaking at 220 rpm, 37 °C. The overnight cultures were then transferred into 10 L of LB containing 100 μg/mL ampicillin and grown at 37 °C with shaking at 220 rpm to OD_{600} of 0.7. L-Arabinose (0.1%) was added to induce the overexpression for 8−10 h at 28 °C. Cells were harvested at 4000 rpm for 30 min at 4 °C, and cell pellets were stored at −80 °C before use.

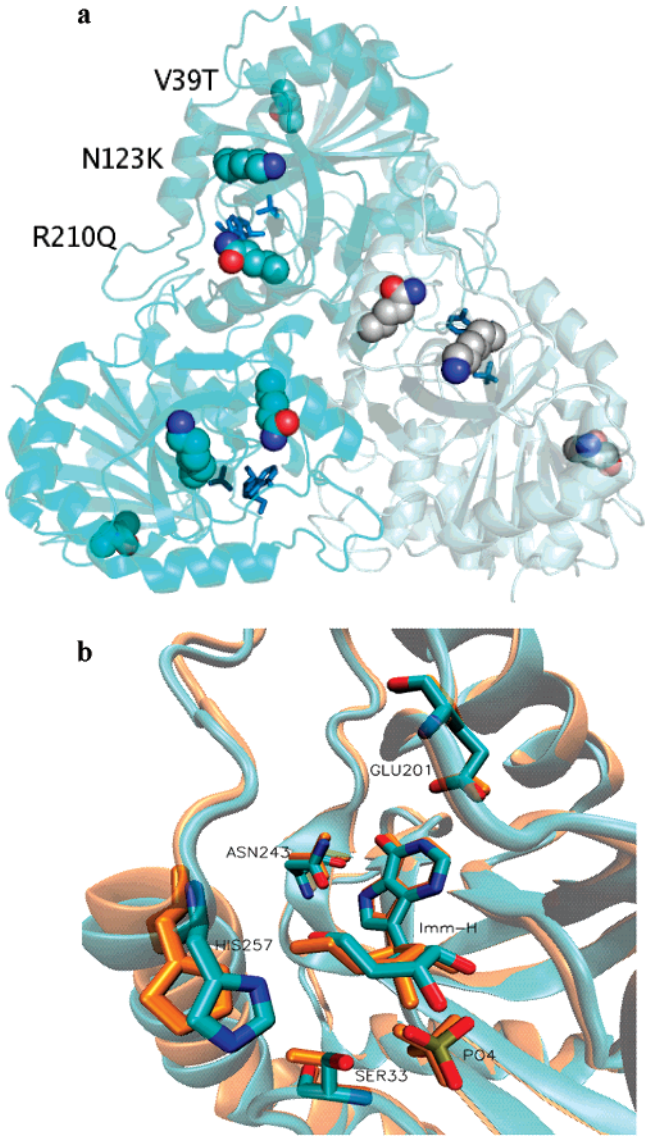

FIGURE 3: Structure of BtPNP showing the location of residues altered to create the triple mutant PNP. (a) The crystal structure of one of the four trimers in the asymmetric unit; the mutations V39T, N123K and R210Q are shown as space-filling models. The monomers are shown in different colors to highlight monomer boundaries. (b) Comparisons of the active sites of HsPNP (PDB ID: 1RR6) in pink and BtPNP (1B8O) in cyan. The figures were created using PyMOL from DeLano Scientific LLC (www.pymol.org). In the figures N is blue, and O is red.

Purification and Protein Concentration Assay. Cells were resuspended in 50 mL of lysis buffer, containing 20 mM

Table 1: Distance from the Active Site of Residues That Are Not Conserved between BtPNP and HsPNP[a]

residue no.	PNP identity		distance from active site (Å)
	bovine	human	
2	Ala	Glu	20.4
12	Asp	Asn	26.1
23	Gln	His	23.5
29	Val	Ile	10.4
39	Val	Thr	13.1
40	Asn	Asp	16.8
93	Phe	Leu	11.9
123	Asn	Lys	14.3
152	Glu	Asp	26.6
210	Arg	Gln	10.8
277	Leu	Ile	19.3

[a] Residues targeted for construction of the chimeric proteins are highlighted. Distance from the active site was a measure of the distance to the nearest point of bound immucillin-H.

$KHPO_4$, pH 7.5, 1 protease inhibitor cocktail tablet and ~10 mg of DNase I. Cells were disrupted by three passes through a French pressure cell. After centrifugation (15,000 rpm for 30 min at 4 °C), the supernatant was applied to a 70 mL Ni-NTA column. Wash buffer (150 mL) containing 10 mM imidazole, 100 mM NaCl and 50 mM $KHPO_4$, pH 7.5 was applied followed by a 10 to 1,000 mM imidazole gradient in the same buffer. The PNPs eluted at approximately 300 mM imidazole. The purified proteins were concentrated, dialyzed against 20 mM Hepes, pH 7.4, 100 mM NaCl and 10% glycerol, and stored at −80 °C, where they are stable for more than 1 year. The PNP concentrations were determined at 280 nm (extinction coefficient of 29.9 mM^{-1} cm^{-1}, calculated by the ExPaSy ProtParam Tool, us.expasy.org (*10*)).

Synthesis of Radiolabeled Inosines. [1′-^{3}H]ATP, [1′-^{14}C]-ATP, [2′-^{3}H]ATP, [5′-^{3}H]ATP, [5′-^{14}C]ATP, were synthesized from [1′-^{3}H]ribose, [1′-^{14}C]ribose, [2′-^{3}H]ribose, [6′-^{14}C]glucose and [6′-^{3}H]glucose-6-phosphate, respectively (American Amersham). [9-^{15}N, 1′-^{14}C]ATP was synthesized from [9-^{15}N]adenine and [1′-^{14}C]ribose. [9-^{15}N, 5′-^{14}C]ATP was synthesized from [9-^{15}N]adenine and [6′-^{14}C]glucose. The chemical synthesis procedures have been reported previously (*1*, *2*, *8*, *11*, *12*). Isotopically labeled [1′-^{3}H]-inosine, [1′-^{14}C]inosine, [2′-^{3}H]inosine, [5′-^{3}H]inosine, [9-^{14}N,1′-^{14}C]inosine and [9-^{14}N,5′-^{14}C]inosine were synthesized from the corresponding ATP molecules using the procedure described previously (*4*).

Steady-State Kinetic and Pre-Steady-State Kinetic Studies. Initial rate studies were performed for the mutant and wild type enzymes using a xanthine oxidase coupled assay (*13*, *14*). Initial rates were measured at pH 7.5, 50 mM Na_2HPO_4 buffer, as a function of inosine concentration (0.5−10 K_m) at 25 °C. The formation of uric acid was monitored at 293 nm using the published molar extinction coefficient of 12,-900 M^{-1} cm^{-1} (*15*). Pre-steady-state kinetic studies were carried out using an Applied Photophysics stopped flow spectrophotometer (model π*−180 spectrometer) equipped with a thermostated water bath. Equal volumes of ~4 μM enzyme in 50 mM KH_2PO_4 pH 7.4 and ~2 mM guanosine were rapidly mixed, and the fluorescence increase caused by enzyme-bound guanine was monitored above 290 nm while exciting at 280 nm. The temperature was varied from 4 °C to 20 °C. Two hundred data points were collected within 0.1 to 0.5 s at each temperature in triplicates. The single turnover rates at different temperatures were calculated by fitting the stopped-flow traces to the single-exponential decay equation (eq 1), where k_{obs} represents the first-order rate constant of the chemical step (the conversion of PNP:guanosine:PO_4 to PNP:guanine:R-1-P, Figure 3), F_t is the fluorescence emission intensity at 290 nm at time t, A is the amplitude of the total change and F_∞ is the fluorescence intensity at infinite time. The temperature dependence of the

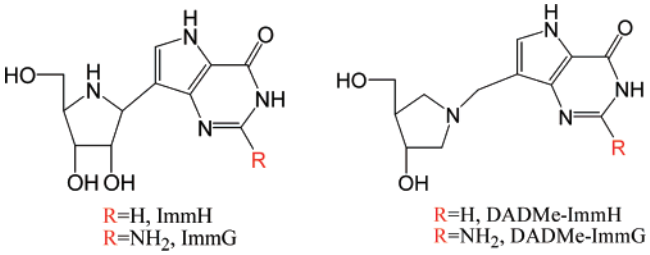

FIGURE 4: Chemical structures of ImmH, ImmG, DADMe-ImmH and DADMe-ImmG. In solution the molecules are cations at neutral pH due to protonation of the nitrogen in the ribosyl mimic.

$$F_t = A^{(-k_{obs}t)} + F_\infty \quad (1)$$

single turnover rate was determined by fitting the data with the Arrhenius and Eyring equations (eq 2 and eq 3, respectively), where k_B and h are the Boltzmann and Planck constants, respectively, A is the preexponential factor, E_a is activation energy, R is the gas constant (8.31 J mol^{-1} K^{-1}) and T is the temperature in kelvins. The enthalpy of activation ($\Delta H^{\ddagger}$) is calculated from the slope of the plots, whereas the entropy ($\Delta S^{\ddagger}$) is calculated from y-intercepts of the plots.

$$\ln(k) = \ln A - [E_a/RT] \quad (2)$$

$$\ln(k/T) = \ln(k_B/h) + \Delta S^{\ddagger}/R - \Delta H^{\ddagger}/RT \quad (3)$$

Inhibition Studies. Slow onset inhibition was measured by the addition of enzyme to reaction mixtures containing 1 mM inosine, 50 mM Na_2HPO_4 pH 7.5 with varied inhibitor concentrations (typically 1 nM to 1 μM) at 25 °C (Figure 4). Inhibitor concentrations were determined spectrophotometrically using the molar extinction coefficients of 9540 M^{-1} cm^{-1} at 261 nm and 8920 M^{-1} cm^{-1} at 269 nm for 9-deaza-inosine (ImmH based inhibitors) and 9-deazaguanosine (ImmG based inhibitors), respectively (*16*). For analysis of slow onset tight-binding inhibition, the lowest inhibitor concentration is usually >10 times the total enzyme concentration (*17*). In conditions where inhibitor concentration does not exceed ten times the enzyme concentration, the effective inhibitor concentration was obtained by the expression

$$I' = I - \left(1 - \frac{V'_0}{V_0}\right)Et \quad (4)$$

where I' is the effective inhibitor concentration, V'_0 and V_0 are the initial rate in the presence and absence of inhibitor, and E_t is the total enzyme concentration (*17*, *18*). The K_i and K_i* (initial and equilibrium dissociation constants) values were determined by fitting the initial reaction rate or the

equilibrium reaction rate and inhibitor concentrations to the following expression for competitive inhibition:

$$\frac{V'_0}{V_0} = \frac{K_m + [S]}{K_m\left(1 + \frac{[I]}{K_i}\right) + [S]} \quad (5)$$

where V'_0 is the initial reaction rate or the equilibrium reaction rate in the presence of inhibitor, and V_o is the initial rate in the absence of inhibitor, [I] is the inhibitor concentration, and [S] is the substrate concentration, which is held at saturating level (1 mM). The dissociation constants of ImmH, ImmG, DADMe-ImmH and DADMe-ImmG were obtained for native and mutant enzymes.

Kinetic Isotope Effects. The KIEs were measured for the arsenolysis of inosine as previously reported (*2*, *4*, *7*, *19*, *20*). Briefly, reaction mixtures contained 100 mM sodium arsenate, 50 mM Tris-HCl (pH 7.5), 250 μM inosine (including label) in 1 mL. 100 μL of the reaction mixture was resolved on charcoal-cellulose columns, and the radioactive ribose was eluted with 3 mL of 20 mM D-ribose containing 10% ethanol (v/v). All fractions from the columns were collected, dried overnight (speedvac), dissolved in 200 μL of water and 20 mL of scintillation fluid and counted for at least 9 cycles at 10 min per cycle.

^{3}H and ^{14}C counts were computed by dual channel counting. Channel 1 was ^{3}H and ^{14}C, while channel 2 was only ^{14}C. The total ^{3}H and ^{14}C were calculated by eq 6 and eq 7, respectively.

$$^3\text{H(total)} = {}^3\text{H(channel 1)} - {}^{14}\text{C(channel 2)}r(^{14}\text{C}) \quad (6)$$

$$^{14}\text{C(total)} = {}^{14}\text{C(channel 2)} + {}^{14}\text{C(channel 2)}r(^{14}\text{C}) \quad (7)$$

where $r(^{14}\text{C})$ is the fraction of ^{14}C counts in channel 1.

The KIEs calculated from the ^{3}H/^{14}C ratios for both partial and complete reactions were corrected to the 0% reaction condition using eq 6:

$$\text{KIE} = \frac{\ln(1-f)}{\ln\left[1 - f\left(\frac{R_f}{R_0}\right)\right]} \quad (8)$$

where f is the fraction of completion of the reaction, and R_f and R_0 are the ratios of heavy to light isotopes at partial and complete conversion, respectively.

Forward Commitment Factor. The method of Rose was used to measure the forward commitment to catalysis (*21*). Reaction mixtures of 10 μL, containing 30 μM PNP in 50 mM Tris-HCl, pH 7.5 and 150 μM [1′-^{14}C]inosine, were incubated for 10 s at room temperature and then diluted with 140 μL of 50 mM inosine and arsenate from 0 to 100 mM. The reactions were quenched after 2 s by adding 50 μL of 1 M HCl. 200 μL of the reaction mixture was resolved on charcoal-cellulose columns, and the radioactive ribose was eluted as described above. Scintillation fluid (20 mL) was added directly to the eluate, and the radioactivity was counted. The forward commitment (C_f) to catalysis was calculated from the fraction of bound inosine converted to product divided by the fraction of bound inosine escaping prior to catalysis at saturating arsenate (as in *19*).

Table 2: Steady-State Kinetic Parameters of the Native and Mutant PNPs[a]

enzyme	K_m (μM)	k_{cat} (s^{-1})	k_{cat}/K_m (M^{-1} s^{-1})
native Hs	40 ± 6	56 ± 6	1.4×10^6
native Bt	32 ± 4	44 ± 2	1.4×10^6
triple mutant Bt	38 ± 7	38 ± 3	1.0×10^6
double mutant Bt	39 ± 6	25 ± 4	0.6×10^6

[a] Values are for the phosphorolysis of inosine.

The intrinsic kinetic KIEs (KIE_{int}) are calculated from the experimental KIEs (KIE_{exp}) and forward commitment factor (C_f) using Northrop's equation (eq 9) (*22*).

$$\text{KIE}_{exp} = \frac{\text{KIE}_{int} + C_f}{1 + C_f} \quad (9)$$

Computational Modeling of PNP Transition State. The transition state for the phosphorolysis of inosine was calculated *in vacuo* using hybrid density functional methods implemented in Gaussian 98 (*23*). The optimization process for the transition state stabilized by PNP was started by varying bond distances between leaving hypoxanthine or nucleophilic phosphate and the C1 of inosine. The structures of inosine (substrate), α-D-ribose 1-phosphate (product) and transition state were optimized using the B3LYP functional and the 6-31G (d, p) basis set. Bond frequencies for the substrate and the transition state were calculated using the same level of theory. All vibrational modes were used for calculating kinetic isotope effects using the ISOEFF98 program (*24*). Frequencies of the substrate, the transition state and a reaction-coordinate imaginary frequency of 50i cm^{-1} or greater were used as the inputs. The KIEs calculated by this procedure were compared with the intrinsic KIEs obtained experimentally to give the transition-state structure most closely representing the intrinsic KIEs.

RESULTS AND DISCUSSION

A goal of this study is to understand how bovine and human PNPs stabilize distinct transition states despite crystallographically conserved catalytic sites. Dynamic contributions from the protein architecture remote from the catalytic sites are implicated and were explored by mutating residues that (1) differ between human and bovine enzymes and (2) are neither surface nor catalytic site residues. Site-directed mutagenesis changed Val39Thr, Asn123Lys, and Arg210Gln in BtPNP to make the structure more similar to HsPNP. Steady-state and pre-steady-state kinetic studies were used to characterize the mutant enzymes. Kinetic isotope effects were measured to determine the effect of the substitutions on the transition-state structure. Altered transition-state structure was additionally validated by altered dissociation constants with transition-state analogues.

Steady-State and Pre-Steady-State Kinetics. Steady-state kinetic parameters showed only small changes in k_{cat} and K_m for the double and triple mutant enzymes, compared to the native HsPNP and BtPNP (Table 2). Since the rate-limiting step of PNPs is release of purine base, changes in the transition-state structure may not be reflected in steady-state kinetics.

Pre-steady-state kinetic studies with guanosine provide a convenient spectral probe since enzyme-bound guanine

Table 3: Pre-Steady-State Kinetic Parameters[a]

parameters	HsPNP	BtPNP	triple mutant BtPNP
k_3 (s^{-1}, 25 °C)[b]	154	316	66
$T\Delta S^{\ddagger}$ (kJ mol^{-1})	17 ± 1	9 ± 1	4.8 ± 0.3
$\Delta H^{\ddagger}$ (kJ mol^{-1})	78 ± 3	67 ± 3	67 ± 3
E_a (kJ mol^{-1})	80 ± 3	70 ± 3	70 ± 3
$\Delta G^{\ddagger}$ (kJ mol^{-1})	60 ± 4	58 ± 3	63 ± 3

[a] Values are for the phosphorolysis of inosine. [b] Values are obtained by extrapolating the Arrhenius plots from lower temperatures since rates are too fast to measure at 25 °C for the HsPNP and BtPNP.

Table 4: Inhibition Constants (pM) of the Native and Mutant PNPs[a]

	DADMe-ImmH	ImmH	DADMe-ImmG	ImmG
native Hs	8.5 ± 0.2	88 ± 3	2 ± 0.2	9.3 ± 0.3
native Bt	100[b]	23[c]	4.7 ± 0.6	26 ± 2
triple mutant Bt	10 ± 1	60 ± 11	11 ± 2	35 ± 1
double mutant Bt	56 ± 8	462 ± 13	8 ± 1	40 ± 7

[a] Inhibition on the initial reaction rate (K_i) is too short to quantitate. The final, tight-binding dissociation constants are reported here. [b] From ref *5*. [c] From ref *14*.

shows strong fluorescence (the conversion of PNP:guanosine:PO_4 to PNP:guanine:R-1-P). The single turnover rate (k_{chem}) of guanosine was obtained at different temperatures for the triple mutant and parent enzymes (Table 3). The triple mutant has a slower k_{chem} of 66 s^{-1} (25 °C) than the rates of 154 and 316 s^{-1} for HsPNP and BtPNP, respectively. This change in rate and a smaller entropic term for catalysis ($T\Delta S^{\ddagger}$ = 4.8 kJ mol^{-1}) suggests that the active sites of the mutant enzyme have transition-state features altered from both BtPNP and HsPNP (*25*). The activation enthalpy ($\Delta H^{\ddagger}$) of triple mutant PNP is 67 kJ mol^{-1}, unchanged from BtPNP, but smaller than the value of 78 kJ mol^{-1} for HsPNP. Mutations distant from the active site alter both the transition-state barrier ($\Delta G^{\ddagger}$) and its thermodynamic properties (Table 4).

Inhibition Studies. Altered binding to transition state analogue inhibitors (ImmH, DADMe-ImmH, ImmG, and DADMe-ImmG) would be anticipated if transition-state properties have been altered (*5*). BtPNP has an early dissociative transition state and higher affinity for ImmH, while HsPNP has a late dissociative transition state and shows higher affinity for DADMe-ImmH. The transition-state structures established for HsPNP use inosine as the substrate, which ImmH and DADMe-ImmH mimic.

Both double and triple mutant enzymes exhibited higher affinity for DADMe-ImmH than for ImmH, suggesting that the transition states of the mutant enzymes are more dissociative than that of their parent enzyme, and more closely resemble HsPNP (Table 4). Triple mutant BtPNP gave K_i* values for DADMe-ImmH and ImmH similar to those of HsPNP, while the double BtPNP has lower affinity for both inhibitors. Thus, mutation of residues Asn123Lys and Arg210Gln alters interactions with transition-state analogues of BtPNP, and mutation of three residues alters BtPNP to be more like HsPNP. Both double and triple mutant BtPNPs show small decreases in affinity for ImmG and DADMe-ImmG, and both enzymes prefer DADMe-ImmG to ImmG. According to X-ray structures of BtPNP with immucillin-H and immucillin-G bound at the catalytic sites, the 9-deazaguanine group alters the position and H-bond contacts between inhibitors and Glu201 (see below). These contacts are proposed to be perturbed by the introduction of the mutations, thus causing decreased K_i* values for inhibitors containing 9-deazaguanine.

Table 5: Experimental and Intrinsic Kinetic Isotope Effects of the Triple Mutant BtPNP

position	exptl[a]	intrinsic[b]	calcd
9-^{15}N	1.019 ± 0.005	1.025 ± 0.005	1.027
1′-^{14}C	1.027 ± 0.006	1.035 ± 0.006	1.033
1′-^{14}C, 9-^{15}N	1.048 ± 0.005	1.063 ± 0.005	1.061
1′-^{3}H	1.168 ± 0.006	1.221 ± 0.006	1.298
2′-^{3}H	1.055 ± 0.002	1.073 ± 0.003	1.057
5′-$^{3}H_2$	1.047 ± 0.002	1.062 ± 0.002	1.101 (proR and S) 1.024 (proR) 1.075 (proS)

[a] Experimental KIEs are corrected to 0% substrate depletion. [b] Intrinsic KIEs are corrected for the forward commitment.

Experimental Kinetic Isotope Effects. KIEs for the triple mutant BtPNP were measured on the arsenolysis of inosine to solve the transition-state structure under the conditions used earlier for BtPNP and HsPNP. The product, ribose 1-arsenate, is unstable and hydrolyzes to ribose and arsenate, which renders the reaction physiologically irreversible (*26*). The apparent KIEs for [1′-^{3}H], [1′-^{14}C], [2′-^{3}H], [5′-^{3}H], [9-^{15}N] and [1′-^{14}C, 9-^{15}N] with the triple mutant enzyme were measured by the competitive radiolabeled method (Table 5). [5′-^{14}C]Inosine was used as a remote control for measuring [1′-^{3}H], [2′-^{3}H] and [5′-^{3}H] isotope effects, and [5′-^{3}H]inosine was used as a remote label to measure [1′-^{14}C], [9-^{15}N] and [1′-^{14}C, 9-^{15}N] KIEs. The remote ^{14}C KIE is assumed to be unity since 5′-^{14}C is three bonds away from the reaction center and ^{14}C is not sensitive to geometric variation in the transition state. [5′-^{3}H], however, gave a 5% KIE for the triple mutant enzyme, similar to that reported for HsPNP (*4*). The [5′-^{3}H] arises from C5′−H5′ bond geometric changes between unbound substrate and the enzyme-bound transition state and includes the dihedral angle H(O)5′−O5′−C5′−H5′ (*7*). The experimental [1′-^{14}C], [9-^{15}N] and [1′-^{14}C, 9-^{15}N] KIEs were then corrected for the [5′-^{3}H] KIE to give 1.028, 1.020 and 1.053, respectively.

Commitment Factor. Forward commitment to catalysis is defined as the ratio of rate constants for product formation to substrate released from the Michaelis complex (*21*, *22*). The forward commitment of the triple mutant BtPNP is 0.243 ± 0.026, slightly greater than for BtPNP and HsPNP (0.19 and 0.15, respectively). The intrinsic KIEs were calculated by correcting the observed KIEs for the forward commitment (Table 5). The intrinsic KIEs for triple mutant BtPNP are similar to those for HsPNP, with the exception of the [1′-^{14}C] KIE (Figure 5). Since intrinsic KIEs are related to bond geometry at the transition state, triple mutant BtPNP is characterized by a different transition state from the native enzyme.

Intrinsic [9-^{15}N], [1′-^{14}C], and [1′-^{14}C, 9-^{15}N] KIEs. The primary [9-^{15}N] KIE reports on the C1′−N9 bond order, protonation of the purine ring and aromatic bond rehybridization of hypoxanthine at the transition state. A large [9-^{15}N] KIE of 1.025 was obtained for the triple mutant BtPNP, close to the KIE for HsPNP (1.029). It suggests that dissociation of the N-glycosidic bond is complete and N7 is protonated at the transition state (*4*, *9*, *19*). The primary [1′-^{14}C] is also informative for determining the nucleophilic participation in

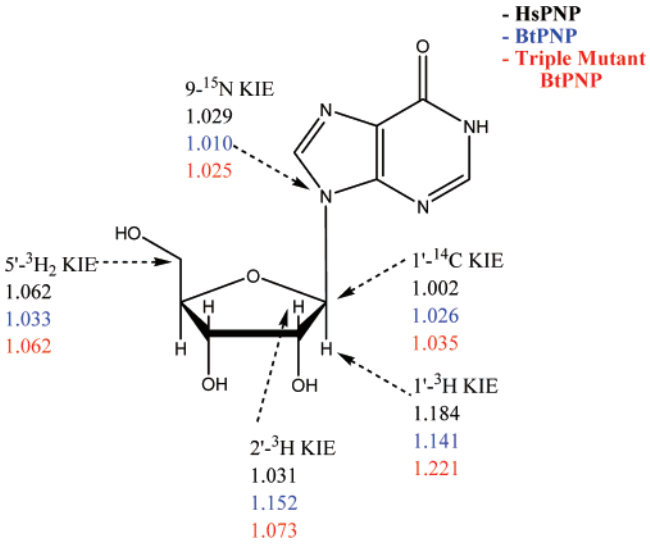

FIGURE 5: Intrinsic kinetic isotope effects for inosine arsenolysis catalyzed by human, bovine and the triple mutant enzyme. The intrinsic KIEs of human and bovine PNPs have been reported previously (*2*, *4*). The KIEs of human PNP are in black, the KIEs of bovine PNP are in blue and the KIEs of the triple mutant enzyme are in red.

substitution reactions. In the case of HsPNP, a [1′-^{14}C] KIE of unity is obtained, indicating a late dissociative S_N1 transition state without nucleophile participation. For BtPNP, the intrinsic [1′-^{14}C] KIE was 1.026 and the [9-^{15}N] KIE was small, suggesting an early dissociative S_N1 transition state (*2*, *4*, *9*, *19*). For the triple mutant BtPNP, the intrinsic [1′-^{14}C] KIE (1.035) is greater than that for either HsPNP or BtPNP. Considering the large [9-^{15}N] KIE obtained for the triple mutant BtPNP, an S_N1 transition state with significant bond order to the phosphate nucleophile is likely (*9*, *19*). The [1′-^{14}C, 9-^{15}N] double KIE can be used to test the consistency of the individually measured [1′-^{14}C] KIE and [9-^{15}N] KIE and to establish that they occur in the same step. The value of the [1′-^{14}C, 9-^{15}N] KIE should be equal to the product of the [1′-^{14}C] KIE and the [9-^{15}N] KIE, and the measured value (1.060) is in good agreement with the calculated value (1.061).

[1′-^{3}H], [2′-^{3}H] and [5′-^{3}H] KIEs. The triple mutant BtPNP exhibits a larger [1′-^{3}H] KIE (1.221) than native HsPNP or BtPNP (1.184 and 1.141, respectively). [1′-^{3}H] KIE gives information on the hybridization of C1′. The KIE increases as the bending frequencies for the out-of-plane bending modes of C1′−H1′ decrease. It is also sensitive to the C1′−N9 distance and to nucleophilic participation at C1′ (*4*, *9*, *19*). The large [1′-^{3}H] KIE of the triple mutant BtPNP is consistent with full loss of the N-ribosidic bond and an early associative transition state with weak nucleophilic phosphate participation at C1′ (*19*). The [2′-^{3}H] KIE is influenced by the positive hyperconjugation of σ(C2′−H2′) bonding electrons to a partially empty $2p_z$ orbital on the anomeric carbon at the transition state, which occurs at specific dihedral angles (H2′−C2′−C1′−N9). Small [2′-^{3}H] KIE suggests significant association of the leaving group, nucleophile participation or unfavorable dihedrals at the transition state, while a large [2′-^{3}H] KIE is indicative of complete dissociation of the leaving group, insignificant nucleophile participation and a favorable dihedral angle. The [2′-^{3}H] KIE of 1.073 for triple mutant BtPNP is moderate and matches a transition-state structure with C1′−O^{phosphate} distance equal to 2.40 Å when the dihedral to the leaving group is most favorable. Since the dihedral angle at the transition state is unknown, the [2′-^{3}H] KIE establishes significant ribooxacarbenium character at the transition state and that the dihedral to the leaving group is partially or fully aligned and is not near a perpendicular to the vacant orbital to the leaving group.

The remote [5′-$^3H_2$] KIE is normally expected to be unity in *N*-ribosyltransferases, since the 5′-$^3H_2$ is four bonds away from the reaction center. However, a large [5′-$^3H_2$] KIE has been observed for human, bovine, and *Plasmodium* PNPs (*2*, *4*, *7*, *19*). Significant distortions in the vibrational modes of the 5′-hydrogens are required to generate the [5′-$^3H_2$] KIE and originate primarily from 5′-hydroxyl dihedral angle anchoring at the transition state (*7*). Computational modeling indicates that isotope effects as large as 10% can be caused by altering the O5′−C5′−C4′−O4′ dihedral angle from −55° for free inosine to 60° at the transition state. The triple mutant BtPNP is similar to the human protein with a large [5′-$^3H_2$] KIE of 1.062. Thus, the triple mutant BtPNP has similar geometrical distortion at C5′ as does the human PNP.

Transition-State Structure. The transition-state structure of the triple mutant BtPNP was optimized at the B3LYP/6-31G (d, p) level of theory by systematically varying N-ribosidic and O^{phosphate}-ribosidic bond distances as well as the 2′-C-*exo/endo* geometry. The calculated transition-state structure of the triple mutant BtPNP has the N-ribosidic bond completely broken (C1′−N9 distance ≥ 3.0 Å) in the transition state. There is nucleophilic phosphate participation at C1′ with C1′−O^{phosphate} = 2.26 ± 0.02 Å. N7 of the leaving group hypoxanthine is fully protonated, and the ribosyl pucker ring adopts a 2′-C-exo conformation (Figure 6 in ref *19*). This transition state is within experimental error of that reported for the K22E:H104R mutant of human PNP (*19*).

Reactions with an intermediate have two transition states, and in two-transition-state systems (in the case of PNPs, N-ribosidic bond breaking, carbocation intermediate and phosphate attack) both transition states can contribute to intrinsic KIEs when their energetic barriers are similar (*27*). The value of the [1′-^{14}C] KIE is greater with triple mutant BtPNP than for HsPNP or native BtPNP and together with the relatively large [9-^{15}N] KIE indicates that the phosphate attack contributes to the transition state. This transition state lies near product on the reaction coordinate since phosphate attack has begun and N-ribosidic bond breaking is complete.

With the exception of the [1′-^{14}C] KIE, the triple mutant BtPNP exhibited KIEs more similar to those of the human than to native bovine PNP. Transition-state analysis reveals that the triple mutant BtPNP has a transition state later in the reaction coordinate than native BtPNP and even later in the reaction coordinate than HsPNP, demonstrating significant nucleophilic participation at C1′.

Although the literature is replete with examples of kinetic properties being altered by remote mutations, this work is a departure from other transition-state analyses in demonstrating that three residues more than 11 Å from the active site can alter the BtPNP transition state to be more like HsPNP with little change of the steady-state kinetic parameters. Remote mutations may alter H-bond patterns that could couple conformational or dynamic changes into the catalytic site and thereby change the transition-state structure. This

work is consistent with the hypothesis that mutation of BtPNP toward HsPNP has altered the transition-state structure by changing the dynamics of the protein, or by mechanisms linked to transition-state conformational changes or by altered pK_a values of groups linked to the catalytic site. The results demonstrate a surprising malleability of enzymatic transition-state structure while maintaining the catalytic rate enhancement.

CONCLUSION

Residues 39, 123 and 210 of BtPNP are more than 11 Å away from the active site and differ substantially between human and bovine PNPs. Mutant enzymes were obtained by mutating two or three of these residues in BtPNP to their counterparts from HsPNP. Steady-state kinetic studies showed only small differences between the mutant and parental enzymes, although pre-steady-state kinetic studies yielded a slower k_{chem} for the triple mutant BtPNP. Changes in the triple mutant BtPNP transition state were suggested by altered affinity to DADMe-ImmH, which mimics the transition-state structure of HsPNP. Transition-state analysis from KIEs and computational chemistry established that the triple mutant BtPNP has a transition-state structure with the N-ribosidic bond completely broken and significant nucleophilic attack at C1′. The energy barrier of nucleophilic attack is higher than it is in human PNP, which defines this step as the primary transition-state barrier and slows the chemical step. The transition-state structure for triple mutant BtPNP is much later in the reaction coordinate than for native BtPNP and is even later that the fully (or equilibrating) S_N1 transition state of HsPNP. Mutations of BtPNP toward HsPNP altered the transition-state structure to be more like the human enzyme. Even remote amino acids contribute to the transition-state structure of PNPs, likely through dynamic motions that form the transition state.

ACKNOWLEDGMENT

The authors thank Drs. Peter Tyler, Richard Furneaux, and Gary B. Evans of Industrial Research, Ltd. (Lower Hutt, New Zealand) for synthesis of DADMe-ImmH, DADMe-ImmG, ImmH and ImmG.

SUPPORTING INFORMATION AVAILABLE

Table of transition state structure data. This material is available free of charge via the Internet at http://pubs.acs.org.

REFERENCES

1. Kline, P. C., and Schramm, V. L. (1992) Purine nucleoside phosphorylase. Inosine hydrolysis, tight binding of the hypoxanthine intermediate, and third-the-sites reactivity, *Biochemistry 31*, 5964−5973.
2. Kline, P. C., and Schramm, V. L. (1993) Purine nucleoside phosphorylase. Catalytic mechanism and transition-state analysis of the arsenolysis reaction, *Biochemistry 32*, 13212−13219.
3. Kline, P. C., and Schramm, V. L. (1995) Pre-steady-state transition-state analysis of the hydrolytic reaction catalyzed by purine nucleoside phosphorylase, *Biochemistry 34*, 1153−1162.
4. Lewandowicz, A., and Schramm, V. L. (2004) Transition state analysis for human and *Plasmodium falciparum* purine nucleoside phosphorylases, *Biochemistry 43*, 1458−1468.
5. Taylor Ringia, E. A., Tyler, P. C., Evans, G. B., Furneaux, R. H., Murkin, A. S., and Schramm, V. L. (2006) Transition state analogue discrimination by related purine nucleoside phosphorylases, *J. Am. Chem. Soc. 128*, 7126−7127.
6. Taylor Ringia, E. A., and Schramm, V. L. (2005) Transition states and inhibitors of the purine nucleoside phosphorylase family, *Curr. Top. Med. Chem. 5*, 1237−1258.
7. Murkin, A. S., Birck, M. R., Rinaldo-Matthis, A., Shi, W., Taylor, E. A., Almo, S. C., and Schramm, V. L. (2007) Neighboring group participation in the transition state of human purine nucleoside phosphorylase, *Biochemistry 46*, 5038−5049.
8. Merkler, D. J., Kline, P. C., Weiss, P., and Schramm, V. L. (1993) Transition-state analysis of AMP deaminase, *Biochemistry 32*, 12993−13001.
9. Singh, V., and Schramm, V. L. (2006) Transition-state structure of human 5′-methylthioadenosine phosphorylase, *J. Am. Chem. Soc. 128*, 14691−14696.
10. Gasteiger E., H. C., Gattiker A., Duvaud S., Wilkins M. R., Appel R. D., Bairoch A. (2005) Protein identification and analysis tools on the ExPASy server, in *The Proteomics Protocols Handbook* (Walker, J. M., Ed.), pp 571−607, Humana Press.
11. Rising, K. A., and Schramm, V. L. (1994) Enzymatic synthesis of NAD^+ with the specific incorporation of atomic labels, *J. Am. Chem. Soc. 116*, 6531−6536.
12. Parkin, D. W., Leung, H. B., and Schramm, V. L. (1984) Synthesis of nucleotides with specific radiolabels in ribose. Primary ^{14}C and secondary ^3H kinetic isotope effects on acid-catalyzed glycosidic bond hydrolysis of AMP, dAMP, and inosine, *J. Biol. Chem. 259*, 9411−9417.
13. Lewandowicz, A., Shi, W., Evans, G. B., Tyler, P. C., Furneaux, R. H., Basso, L. A., Santos, D. S., Almo, S. C., and Schramm, V. L. (2003) Over-the-barrier transition state analogues and crystal structure with *Mycobacterium tuberculosis* purine nucleoside phosphorylase, *Biochemistry 42*, 6057−6066.
14. Miles, R. W., Tyler, P. C., Furneaux, R. H., Bagdassarian, C. K., and Schramm, V. L. (1998) One-third-the-sites transition-state inhibitors for purine nucleoside phosphorylase, *Biochemistry 37*, 8615−8621.
15. Dawson, R. M. C., Elliott, D. C., Elliott, W. H., and Jones, K. M. (1986) *Data for Biochemical Research*, 3rd ed., Clarendon Press, Oxford.
16. Lim, M.-I., Ren, Y.-Y., Otter, B. A., and Klein, R. S. (1983) Synthesis of "9-deazaguanosine" and other new pyrrolo[3,2-d]-pyrimidine C-nucleosides, *J. Org. Chem. 48*, 780−788.
17. Morrison, J. F., and Walsh, C. T. (1988) The behavior and significance of slow-binding enzyme inhibitors, *Adv. Enzymol. Relat. Areas Mol. Biol. 61*, 201−301.
18. Singh, V., Evans, G. B., Lenz, D. H., Mason, J. M., Clinch, K., Mee, S., Painter, G. F., Tyler, P. C., Furneaux, R. H., Lee, J. E., Howell, P. L., and Schramm, V. L. (2005) Femtomolar transition state analogue inhibitors of 5′-methylthioadenosine/S-adenosylhomocysteine nucleosidase from *Escherichia coli*, *J. Biol. Chem. 280*, 18265−18273.
19. Luo, M., Li, L., and Schramm, V. L. (2008) Remote mutations alter transition-state structure of human purine nucleoside phosphorylase, *Biochemistry 47*, 2565−2576.
20. Gutierrez, J. A., Luo, M., Singh, V. P., Li, L., Brown, R. L., Norris, G. E., Evans, G. B., Furneaux, R. H., Tyler, P. C., Painter, G. F., Lenz, D. H., and Schramm, V. L. (2007) Picomolar inhibitors as transition state probes of 5′-methylthioadenosine nucleosidases, *ACS Chem. Biol. 2*, 725−734.
21. Rose, I. A. (1980) The isotope trapping method: desorption rates of productive E. S complexes, *Methods Enzymol. 64*, 47−59.
22. Northrop, D. B. (1981) The expression of isotope effects on enzyme-catalyzed reactions, *Annu. Rev. Biochem. 50*, 103−131.
23. Frisch, A., Ed. (1999) *Gaussian 98 user's reference*, 2nd ed., Gaussian.
24. Anisimov, V., and Paneth, P. (1999) A program for studies of isotope effects using Hessian modifications, *J. Math. Chem. 26*, 75−86.
25. Ottosson, J., Fransson, L., and Hult, K. (2002) Substrate entropy in enzyme enantioselectivity: an experimental and molecular modeling study of a lipase, *Protein Sci. 11*, 1462−1471.
26. Schramm, V. L. (1999) Enzymatic transition-state analysis and transition-state analogs, *Methods Enzymol. 308*, 301−355.
27. McCan, J. A. B., and Berti, P. J. (2007) Transition State Analysis of Acid-catalyzed dAMP Hydrolysis, *J. Am. Chem. Soc. 129*, 7055−7064.

BI7021365